

# RV-FuseNet: Range View based Fusion of Time-Series LiDAR Data for Joint 3D Object Detection and Motion Forecasting

Ankit Laddha  
aladdha@uber.com

Shivam Gautam  
sgautam@uber.com

Gregory P. Meyer  
gmeyer@uber.com

Carlos Vallespi-Gonzalez  
cvallespi@uber.com

Uber Advanced Technologies Group  
Pittsburgh, USA

---

## Abstract

Autonomous vehicles rely on robust real-time detection and future motion prediction of traffic participants to safely navigate urban environments. We present a novel end-to-end approach that uses raw time-series LiDAR data to jointly solve both detection and prediction. We use the range view representation of LiDAR instead of voxelization since it does not discard information and is more efficient due to its compactness. However, for time-series fusion the data needs to be projected to a common viewpoint, and often this viewpoint is different from where it was captured leading to distortions. These distortions have an adverse impact on performance. Thus, we propose a novel architecture which reduces the impact of distortions by sequentially projecting each sweep into the viewpoint of the next sweep in time. We demonstrate that our sequential fusion approach is superior to methods that directly project all the data into the most recent viewpoint. Furthermore, we compare our approach to existing state-of-the-art methods on multiple autonomous driving datasets and show competitive results.

## 1 Introduction

Autonomous vehicles need to perform path planning in dense, dynamic urban environments where many actors are simultaneously trying to navigate. This requires robust and efficient methods for object detection and motion forecasting. The goal of detection is to recognize the objects present in the scene and estimate their 3D bounding box. While, prediction aims to estimate the position of the detected boxes in the future. Traditionally, separate models have been used for detection and prediction. In this work, we present a method for jointly solving for both object detection and motion forecasting directly from LiDAR data. As demonstrated previously [9, 14, 18], joint methods benefit from reduced latency, efficient feature sharing across both tasks, lower computational requirements and ease of maintenance as compared to multi-stage pipelines.

The LiDAR sensor generates measurements using a stack of rotating lasers, and each measurement provides a range and an angle. Therefore, the LiDAR data is naturally represented by a compact spherical image, which is commonly referred to as a Range View (RV) image. Many previous methods [9, 11, 12, 27] project the data onto a Cartesian grid around the ego-vehicle. However, this Bird’s Eye View (BEV) projection loses the precise point information due to voxelization. Additionally, it loses important context on which parts of the scene are occluded and which parts are empty. Whereas, the RV representation is able to preserve both the point and occlusion information. Due to its efficiency and information preservation benefits [16, 17], we use the RV representation of the LiDAR data.

Each sweep of the of LiDAR only provides the position for each object at any given moment; whereas, higher order states such as velocity, acceleration and intent are required for predictions. Thus, the fusion of sensor data across time becomes paramount for motion forecasting. However, fusing multiple time-steps of sensor data is challenging as the observed world state is non-stationary due to dynamic actors and ego-motion. To decouple object motion and ego-motion, all of the existing end-to-end methods [9, 9, 12, 18] compensate for ego-motion during fusion of temporal data. However, this compensation requires projecting the data into a different viewpoint from which it was captured. In the RV, this projection can create distortions, such as gaps in continuous surfaces, as well as information loss due to self-occlusions, occlusions between objects and discretization effects (see Figure 1). Furthermore, the amount of distortion is dependent on several factors such as the amount of ego-motion, the speed of the objects and the distance of the observed objects from the ego-vehicle. Minimizing these distortions is critical for maximizing the performance on the prediction and detections tasks.

In this paper, we propose a principled way to reduce the impact of distortion caused by change in viewpoint for fusion. We propose to sequentially fuse the temporal LiDAR data by projecting the data collected from one viewpoint to the next in time. We show its effectiveness compared to projecting all the data into the most recent viewpoint [18]. We further demonstrate that the sequential fusion is particularly effective in cases where fast ego-motion or object motion is present. Additionally, we establish new state-of-the-art results for multiple classes of objects on the ATG4D [17] and nuScenes [2] datasets.

## 2 Related Work

Temporal fusion of sensor data is of paramount importance for robust state and motion estimation. The most popular methods of enforcing temporal consistency involve using detection-based approaches [11, 13, 16, 17, 21, 22, 29] to generate object detections followed by stitching across time through object tracking [9, 19, 23, 25]. Even though detect-then-track approaches are widely used for estimating state (i.e. position, velocity and acceleration), such approaches are not suitable for long-term trajectory predictions that are needed to navigate dense, urban environments [4].

The ability to provide a probabilistic method of fusing temporal information using Kalman Filters [26] has inspired the use of learned methods that rely on temporally smoothed filter output to generate long term prediction [5, 7]. Other approaches directly use object detections as input to recurrent networks to implicitly learn actor behavior and predict future trajectories [1, 6, 12, 15, 23]. However, such approaches rely on the output of detection and tracking systems making them susceptible to any changes and errors in the upstream models. For practical applications, this often results in cascaded pipelines which are hard to train, de-

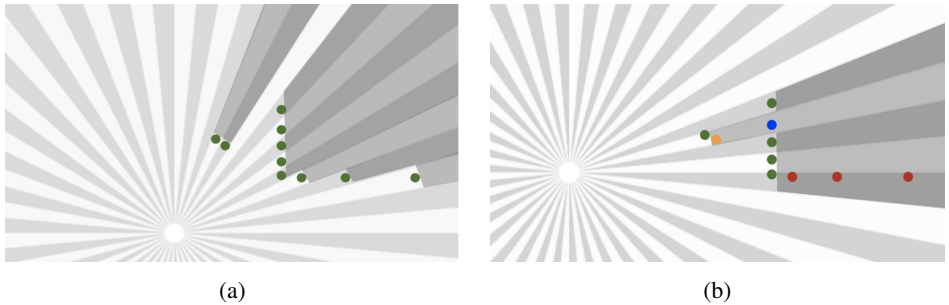


Figure 1: Example of distortions that may arise from changing the viewpoint in the RV. We depict a sweep for a single laser with the scene discretized into angular bins. In Figure 1a, we show the sweep from its original viewpoint, i.e. the viewpoint from which the data was captured. All measurements for two objects are shown in green, and the occluded area behind them is shaded. In Figure 1b, we show the same LiDAR points with a different viewpoint. As a result, we see several types of information loss. While green points are still visible to the sensor, blue points are lost due to occlusions from other objects. Red points are lost due to self-occlusions and yellow points are lost due to multiple points falling into the same bin.

bug and maintain. Further, such approaches lose out on rich feature representations learned by object detection networks.

Another class of learned methods for motion forecasting focus on learning a probability distribution over the future Occupancy of Grid Maps (OGMs) [11, 20, 24]. They replace the multi-stage systems needed for detection and tracking with a single model to predict grid occupancy directly from sensor data. However, OGM based approaches fail to model actor-specific characteristics like class attributes and kinematic constraints. Furthermore, modeling complex interactions among actors and maintaining a balance between discretization resolution and computational efficiency remains a challenge [8].

In contrast to multi-stage and OGM based methods, end-to-end approaches aim at jointly learning object detection and motion forecasting [3, 9, 14, 18, 28]. This eliminates the need for multiple-stages (reducing latency and system complexity) while still preserving actor specific characteristics of the prediction model. In this work we present a method for jointly estimating object detection and future trajectory in an end-to-end manner.

End-to-end methods for motion forecasting can be classified based on the representation they use for feature extraction. As discussed previously, while some methods represent input LiDAR points in the Birds-Eye View (BEV) [3, 9, 14, 28], other methods operate in the native Range View (RV) [18]. The projection of LiDAR points in BEV preserves the size of the actor across time and provides a strong prior to models learning from past temporal data. However, the RV representation is naturally compact, computationally efficient and preserves occlusion information. Due to objects not being scale invariant across time in RV, this representation is prone to distortions. In [18], the authors show how naively projecting past LiDAR sweeps into the current frame can lead to distortions due to self-occlusions and perspective changes.

Learned methods for end-to-end motion forecasting can also be classified based on how they fuse past LiDAR sweeps with the current sweep. Most approaches operate in BEV [3, 14, 28] and transform past sweeps to the current reference frame through a rigid transform. Afterwards, the temporal layers can either be processed through 3D convolutions [14] or by

stacking together and processing through 2D convolutions [4, 28]. We call this approach of using the transformed sensor data as additional channels in the network as ‘‘Early Fusion’’. The only approach that utilizes the RV representation for motion forecasting is LaserFlow [28], which processes each past sweep in its original frame to generate a set of feature maps. The data is then fused together by projecting all the features into a reference frame. We refer this approach as ‘‘Late Fusion.’’ Compared to [28], we propose an ‘‘Incremental Fusion’’ approach that effectively combines the features extracted in the original viewpoint with the next viewpoint in the sequence.

### 3 Approach

As the LiDAR sensor rotates, it continuously generates measurements. The data is sliced into ‘‘sweeps,’’ wherein each slice contains the measurements from a full 360° rotation of the sensor. In order to detect and predict the motion of objects, we utilize features extracted from a sequence of sweeps (Section 3.1) which are projected into the range view representation (Section 3.2). Features from individual sweeps are fused together (Section 3.3), and spatio-temporal features are extracted using a novel network architecture (Section 3.4). Finally, the resulting spatio-temporal features are passed to a backbone network to produce a set of detections and predictions (Section 3.5).

#### 3.1 Multi-Sweep Input

Assume we are given a time-series of  $K$  sweeps denoted by  $\{\mathcal{S}_k\}_{k=0}^{1-K}$  where  $k = 0$  is the most recent sweep and  $-K < k < 0$  are the past sweeps. Each sweep contains a set of  $N_k$  points,  $\mathcal{S}_k = \{\mathbf{p}_k^i\}_{i=0}^{N_k-1}$ , in the coordinate frame defined by the pose or viewpoint of the sensor when the sweep was captured,  $\mathcal{P}_k$ . The pose of the sensor is provided by the autonomous system, so we can calculate the transformation from one sweep to another. We denote the  $m$ -th sweep transformed into the  $n$ -th sweep’s coordinate frame as  $\mathcal{S}_{m,n} = \{\mathbf{p}_{m,n}^i\}_{i=1}^{N_m}$  where each point is represented by its 3D coordinates,  $[x_{m,n}^i, y_{m,n}^i, z_{m,n}^i]^T$ , and the id of the laser,  $l_m^i$ , which produced the measurement.

For each point  $\mathbf{p}_{m,n}^i$ , we can define a set of features, including its range

$$r_{m,n}^i = \|\mathbf{p}_{m,n}^i\| \quad (1)$$

and angle

$$\theta_{m,n}^i = \text{atan2}(y_{m,n}^i, x_{m,n}^i). \quad (2)$$

As input, we use the range and angle in the original coordinate frame,  $r_m^i$  and  $\theta_m^i$ , and the range and angle in the reference frame,  $r_{m,0}^i$  and  $\theta_{m,0}^i$ , as this provides some notation of the ego-motion. Furthermore, if a high-definition map is available, we can compute its height above ground and a flag indicating whether or not the point is on or above a drivable surface.

#### 3.2 Range View Projection

To form a range view image, we define the projection of a point  $\mathbf{p}_{m,n}^i$  as,

$$P(\mathbf{p}_{m,n}^i) = (l_m^i, \lfloor \theta_{m,n}^i / \Delta\theta \rfloor) \quad (3)$$

where the row is specified by the point’s laser id, and the column is determined by its discretized angle. The value of  $\Delta\theta$  is approximately the angular resolution of the LiDAR.

Furthermore, if more than one point happens to project into the same image coordinate, we keep the point with the smallest range,  $r_{m,n}^i$ . By applying the projection to every point in  $\mathcal{S}_{m,n}$ , we can generate a range view image.

### 3.3 Range View Fusion

To fuse the range view images from multiple sweeps, we need to compensate for ego-motion. This is accomplished by projecting the points into a common viewpoint. For example, assume we would like to fuse two sweeps,  $\mathcal{S}_m$  and  $\mathcal{S}_n$ . When fusing multiple sweeps, we always use the viewpoint of the most recently captured sweeps. In this case, let us assume  $n > m$ ; therefore, the pose  $\mathcal{P}_n$  will define the shared coordinate system, and we will transform the  $m$ -th sweep into this coordinate system to generate  $\mathcal{S}_{m,n}$ . Utilizing Eq. 3, we are able to determine the points from each sweep that project into the same image coordinate. Assume  $\mathbf{p}_{m,n}^i$  and  $\mathbf{p}_n^i$  project into the same coordinate, each point will have a corresponding vector of features,  $\mathbf{f}_{m,n}^i$  and  $\mathbf{f}_n^i$ , which are either hand-craft features like the ones described in Section 3.1 or features learned by a neural network. These features describe the surface of an object along the ray emanating from the origin of the coordinate system and passing through  $\mathbf{p}_{m,n}^i$  and  $\mathbf{p}_n^i$ . However, due to object motion, the features could be describing different objects. Therefore, we provide the relative distance between the points as an additional feature,

$$\mathbf{h}_{m,n}^i = \mathbf{R}_{\theta_n^i}[\mathbf{p}_{m,n}^i - \mathbf{p}_n^i] \quad (4)$$

where  $\mathbf{R}$  is a rotation matrix parameterized by the angle  $\theta_n^i$ . The resulting fused features corresponding to the pair of points,  $\mathbf{p}_{m,n}^i$  and  $\mathbf{p}_n^i$ , is  $\mathbf{f}^i = [\mathbf{f}_n^i, \mathbf{f}_{m,n}^i, \mathbf{h}_{m,n}^i]$ . Applying this operation to every point in  $\mathcal{S}_{m,n}$ , we are able to produce a fused range view image. Although we have described the fusion for a pair of sweeps, this procedure can be trivially extended to any number of sweeps.

### 3.4 Multi-Sweep Fusion Architectures

Our proposed fusion method, described in the previous section, requires the projection of LiDAR points into a viewpoint different than the one used to capture the data. As a result, distortions are introduced into the image proportional to the distance between the viewpoints. Therefore, mitigating the effect of distortions is critical. In this section, we propose multiple fusion architectures with the aim of successively preserving more information and minimize the impact of distortions during multi-sweep fusion.

#### 3.4.1 Early Fusion

Figure 2a shows the early fusion architecture. We simply fuse our hand-crafted features from all the sweeps into the viewpoint of the most recent sweep. This introduces a significant amount of distortion since every sweep is directly projected into the most recent viewpoint. To alleviate this problem, we propose the next architecture inspired by [13].

#### 3.4.2 Late Fusion

Figure 2b shows the proposed late fusion architecture. We first build a range view image for each sweep in its own viewpoint using our hand-craft features. Afterwards, we pre-process the images using a light-weight convolution neural network  $CNN_s$ , which provides learned features for each LiDAR point in the image. Subsequently, we fuse all the images into the

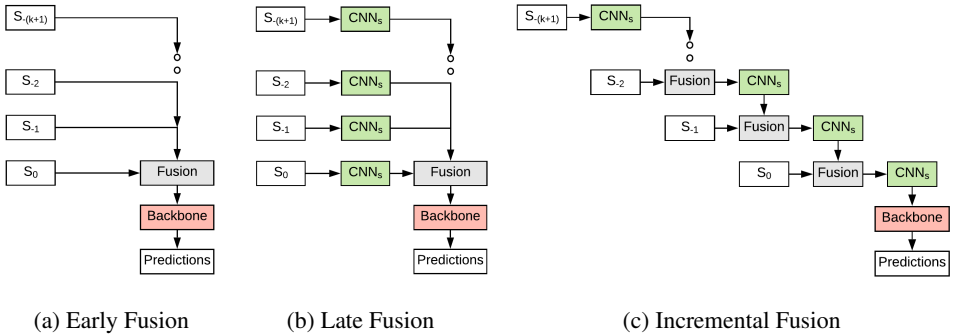


Figure 2: Proposed Multi-Sweep fusion architectures. The colored blocks have learn-able parameters in them. Please refer to section 3.3 for the fusion block and section 3.4 for details on the architectures.

most recent viewpoint. As shown in [18], this reduces the impact of distortions, since the learned features are extracted from the original undistorted images. Since the features are still projected directly into the most recent viewpoint, information loss for farther in time sweeps may still be high. To further mitigate this issue we propose the next architecture.

### 3.4.3 Incremental Fusion

Figure 2c shows the incremental fusion architecture which sequentially fuses the sweeps. Each sweep extracts features from its original viewpoint after being fused with the features from the previous sweep. With this design, sweeps are only projected into its neighboring sweep in time. Since the viewpoint changes slowly with time, this results in only a minimal amount of distortion.

## 3.5 Predictions

After extracting and fusing multi-sweep features using one of our proposed architectures, the resulting feature map will be in the range view corresponding to the viewpoint of the most recent sweep. These features are passed to a backbone network to produce a set of detections and predictions for the current sweep. We utilize the backbone network and predictions proposed by [18]. In the following section, we demonstrate that our proposed fusion architectures can improve both detection and prediction performance.

# 4 Experiments

## 4.1 Datasets and Metrics

We present experimental results on two datasets: ATG4D [17] and nuScenes [2]. These datasets have different LiDAR sensors and are collected in different cities showing the wide applicability of our approach. ATG4D has a higher resolution LiDAR with 64 lasers and nuScenes has 32 lasers. Additionally, the LiDAR in ATG4D has twice the angular resolution of nuScenes. Due to these differences a sweep in ATG4D has 4x more points per sweep than nuScenes.

We use Average Precision (AP) for detection and displacement error at future time-stamps for predictions. AP is computed as the area under the curve for the precision-recall

Method	ATG4D				nuScenes			
	AP (%)	$L_2$ (cm)			AP (%)	$L_2$ (cm)		
	0.7 IoU	0.0 s	1.0 s	3.0 s	0.7 IoU	0.0 s	1.0 s	3.0 s
FaF [14]	64.1	30	54	180	-	-	-	-
IntentNet [9]	73.9	26	45	146	-	-	-	-
NMP [28]	80.5	23	36	114	-	-	-	-
SpAGNN [9]	83.9	22	33	<b>96</b>	-	<b>22</b>	58	145
LaserFlow [18]	84.5	<b>19</b>	31	99	49.7	27	54	153
RV-FuseNet (ours)	<b>84.8</b>	20	<b>30</b>	98	<b>53.5</b>	27	<b>46</b>	<b>123</b>

Table 1: Detection and Motion Forecasting performance on vehicles. Similar to [9], for forecasting comparison, we use a recall of 80% on ATG4D and 60% on nuScenes.

curve. The displacement error is computed as the Euclidean distance between the center of predicted box and the ground truth box. Since each method produces a different set of detections, for a fair comparison we compute the displacement error using the same recall point for all the methods similar to [9].

## 4.2 Implementation Details

The network (CNN<sub>s</sub>) in Figure 2 is used to extract low-level features before fusion with other sweeps. For both late and incremental fusion, we use 3 layers of  $3 \times 3$  convolutions with 32 feature channels each.

The size of the range view image is  $64 \times 2048$  for ATG4D and is  $32 \times 1024$  for nuScenes. Unless otherwise specified, for ATG4D we use a circle with a diameter of 240m, centered on the ego-vehicle, as the Region of Interest (ROI). For nuScenes, we use the official ROI of a square of 100m length centered on the ego-vehicle. We use the LiDAR data from the past 0.5s and predict a trajectory for 3s into the future at 1s intervals. All other training parameters such as learning rate, loss weights, number of iterations are the same as in [18].

## 4.3 Comparison with State of the Art

Table 1 compares our incremental fusion to existing BEV and RV based methods on ATG4D. The computational cost of BEV methods scale linearly with the area required to process. Thus, due to computational constraints, all the BEV methods [9, 4, 14] report results on the reduced ROI of  $140m \times 80m$ . In this experiment, our method outperforms all other methods on the detection task. Additionally, our method outperforms all the single stage methods [9, 14, 18, 28] at all the timestamps and achieve similar performance to a two-stage method SpAGNN [9].

Table 1 also compares our method with LaserFlow [18] and SpAGNN [9] on nuScenes. It is a more challenging dataset than ATG4D due to an order of magnitude less training data and a sparser LiDAR. On this dataset, our method outperforms both of these methods, improving predictions at 3s by more than 15%.

## 4.4 Comparison of Proposed Architectures

The impact of distortions created by changing the viewpoint for fusion is dependent on factors such as the actor speed, ego-vehicle speed and the distance of objects to the most recent viewpoint. We analyze the various architectures over a range of these factors.

Figure 3 shows the percentage improvement of late and incremental fusion over early fusion on the displacement error at 3s. As shown in Figure 3a, we see significant gains with

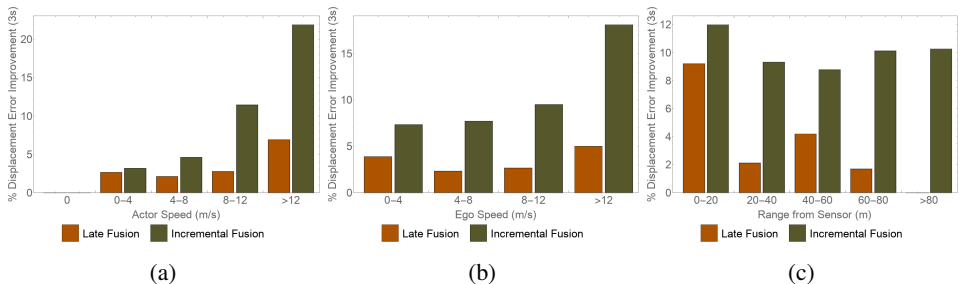


Figure 3: These plots show the relative improvement (%) of the late and incremental fusion architectures over the early fusion on categories that often lead to higher distortions. **3a** shows the relative improvements binned by actor speed, **3b** is binned by ego-vehicle speed and **3c** is binned by range from sensor to object.

Method	Vehicle				Bicycle				Pedestrian			
	AP (%)	$L_2$ (cm)			AP (%)	$L_2$ (cm)			AP (%)	$L_2$ (cm)		
	0.7 IoU	0.0 s	1.0 s	3.0 s	0.5 IoU	0.0 s	1.0 s	3.0 s	0.5 IoU	0.0 s	1.0 s	3.0 s
LaserFlow [18]	74.5	24	38	112	59.1	15	22	50	74.8	12	27	72
RV-FuseNet (Ours)	<b>74.6</b>	<b>24</b>	<b>37</b>	<b>109</b>	56.4	<b>14</b>	<b>18</b>	<b>36</b>	<b>76.6</b>	<b>12</b>	28	74

Table 2: Detection and Motion Forecasting performance on ATG4D.

the incremental fusion architecture as the actor speed increases. This illustrates the effectiveness of the proposed incremental fusion over both early and late fusion approaches in reducing the impact of distortions due to fast moving objects. Stationary objects are usually easy to estimate with only two consecutive sweep. Thus, we see no difference between the architectures on these objects. As a result, for comparisons in Figure 3b and Figure 3c we only use moving objects. The distortions also increase with an increase in the speed of the ego-vehicle. Figure 3b shows improvements of the late and incremental fusion on a range of ego-speed. Again, in this scenario the incremental fusion approach shows greater improvements as ego-vehicle speed increases. Finally, we evaluate the impact of range to the objects in Figure 3c. The objects closer to the LiDAR sensor have high distortions in fusion due to heavy self-occlusions. In this case, as shown in Figure 3c, both late fusion and incremental fusion provide huge improvements over early fusion architecture. Moreover, incremental fusion offers significantly better performance than late fusion in situations where objects are further from the LiDAR sensor, as there the data is sparser and the ability to preserve more information in the fusion blocks is critical.

## 4.5 Comparison on Multi-Class and Larger ROI

We compare our method on multiple classes at the full range of the LiDAR. LaserFlow [18] is the only other method which provides results in this setting and we compare against it in Table 2. Figure 3c shows that incremental fusion gets large improvements over late fusion at longer ranges. Therefore, on vehicles, our method outperforms LaserFlow [18] which is a late fusion method. Additionally, we show a large improvement of 30% on 3s predictions for bicycles. We believe this is due to the fact that bicycles can still move at >12m/s like vehicles, but because of their smaller size they are more vulnerable to information loss due to distortions. Finally, we get similar performance on pedestrians since they are slow moving and in these conditions late fusion and incremental fusion architectures offer similar performance.

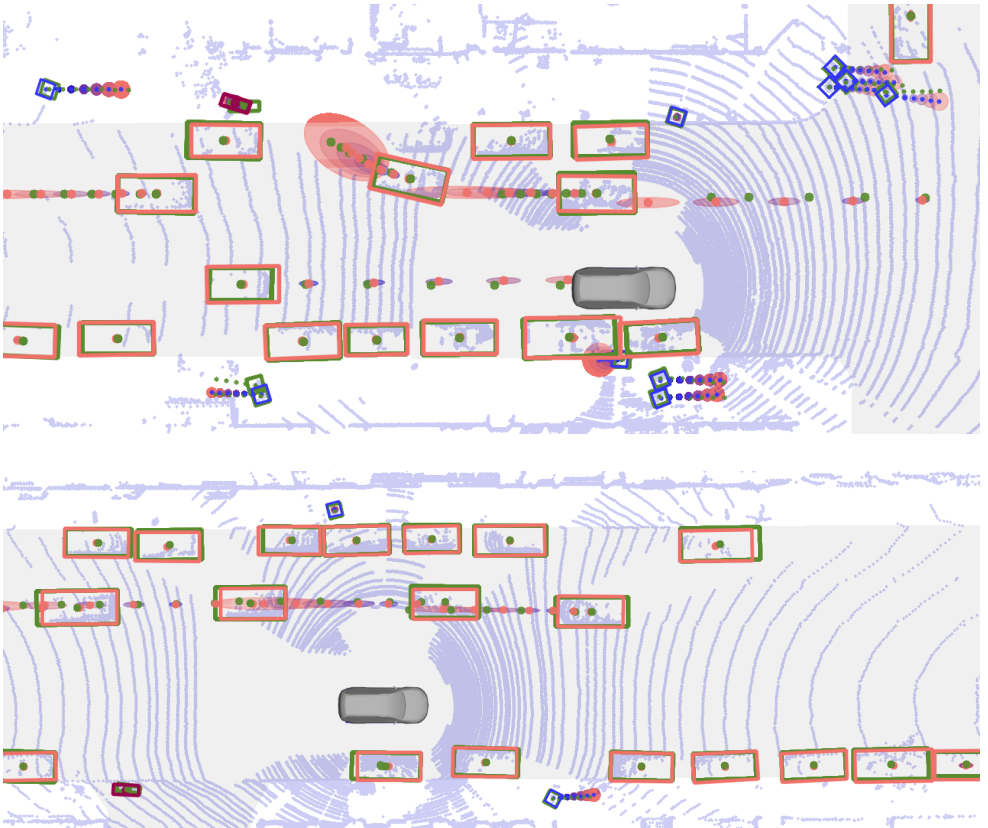


Figure 4: Qualitative result on ATG4D for multiple classes using RV-FuseNet. Vehicle predictions are shown in orange, bicycles are in maroon, and pedestrians are in purple. The ground-truth for each class is depicted in green.

## 4.6 Qualitative Results

We show results of our multi-class model on ATG4D in Figure 4. As in [18], we also predict the future bounding box, but for visualization purposes we only show the center of the box. In addition, we visualize one standard deviation of the predicted trajectory uncertainty at each time-step. These results clearly demonstrate that our model is able to accurately detect and forecast the future position for multiple classes at different range.

## 5 Conclusion

In this work we presented a novel method for joint object detection and motion forecasting using time-series LiDAR data. Our novel incremental fusion approach provides a principled way of fusing multiple LiDAR sweeps which reduces the information loss during fusion. As a result, we show state-of-the-art results for motion forecasting on the ATG4D and the nuScenes datasets. Further, we provide an analysis of our method on scenarios prone to distortion and prove the efficacy of our method in handling such situations over the approach of fusing all the sweeps at once.

As part of our ongoing research, we would like to explore fusing high definition map information, like lanes and traffic lights, in order to incorporate contextual information from the scene. Furthermore, adding information from sensors that directly observe higher order states, such as RADAR, should further improve trajectory prediction. Finally, modeling actor interactions is another potential direction to improve the predictions.

## References

- [1] Alexandre Alahi, Kratarth Goel, Vignesh Ramanathan, Alexandre Robicquet, Li Fei-Fei, and Silvio Savarese. Social LSTM: Human trajectory prediction in crowded spaces. In *Proceedings of the IEEE Conference on Computer Vision and Pattern Recognition (CVPR)*, 2016.
- [2] Holger Caesar, Varun Bankiti, Alex H Lang, Sourabh Vora, Venice Erin Liong, Qiang Xu, Anush Krishnan, Yu Pan, Giancarlo Baldan, and Oscar Beijbom. NuScenes: A multimodal dataset for autonomous driving. *arXiv preprint arXiv:1903.11027*, 2019.
- [3] Sergio Casas, Wenjie Luo, and Raquel Urtasun. IntentNet: Learning to predict intention from raw sensor data. In *Proceedings of the Conference on Robot Learning (CoRL)*, 2018.
- [4] Sergio Casas, Cole Gulino, Renjie Liao, and Raquel Urtasun. Spatially-aware graph neural networks for relational behavior forecasting from sensor data. *arXiv preprint arXiv:1910.08233*, 2019.
- [5] Henggang Cui, Vladan Radosavljevic, Fang-Chieh Chou, Tsung-Han Lin, Thi Nguyen, Tzu-Kuo Huang, Jeff Schneider, and Nemanja Djuric. Multimodal trajectory predictions for autonomous driving using deep convolutional networks. In *2019 International Conference on Robotics and Automation (ICRA)*, pages 2090–2096. IEEE, 2019.
- [6] Nachiket Deo and Mohan M Trivedi. Convolutional social pooling for vehicle trajectory prediction. In *Proceedings of the IEEE Conference on Computer Vision and Pattern Recognition Workshops (CVPRW)*, 2018.
- [7] Nemanja Djuric, Vladan Radosavljevic, Henggang Cui, Thi Nguyen, Fang-Chieh Chou, Tsung-Han Lin, and Jeff Schneider. Motion prediction of traffic actors for autonomous driving using deep convolutional networks. *arXiv preprint arXiv:1808.05819*, 2018.
- [8] E. Einhorn, C. Schr  uter, and H. Gross. Finding the adequate resolution for grid mapping - cell sizes locally adapting on-the-fly. In *2011 IEEE International Conference on Robotics and Automation*, pages 1843–1848, 2011.
- [9] Shivam Gautam, Gregory P. Meyer, Carlos Vallespi-Gonzalez, and Brian C. Becker. Sdvtracker: Real-time multi-sensor association and tracking for self-driving vehicles, 2020.
- [10] Stefan Hoermann, Martin Bach, and Klaus Dietmayer. Dynamic occupancy grid prediction for urban autonomous driving: A deep learning approach with fully automatic labeling. *2018 IEEE International Conference on Robotics and Automation (ICRA)*,

- May 2018. doi: 10.1109/icra.2018.8460874. URL <http://dx.doi.org/10.1109/ICRA.2018.8460874>.
- [11] Alex H. Lang, Sourabh Vora, Holger Caesar, Lubing Zhou, Jiong Yang, and Oscar Beijbom. PointPillars: Fast encoders for object detection from point clouds. In *Proceedings of the IEEE Conference on Computer Vision and Pattern Recognition (CVPR)*, 2010.
- [12] Namhoon Lee, Wongun Choi, Paul Vernaza, Christopher B Choy, Philip HS Torr, and Manmohan Chandraker. DESIRE: Distant future prediction in dynamic scenes with interacting agents. In *Proceedings of the IEEE Conference on Computer Vision and Pattern Recognition (CVPR)*, 2017.
- [13] Bo Li, Tianlei Zhang, and Tian Xia. Vehicle detection from 3D lidar using fully convolutional network. In *Proceedings of Robotics: Science and Systems (RSS)*, 2016.
- [14] Wenjie Luo, Bin Yang, and Raquel Urtasun. Fast and furious: Real time end-to-end 3D detection, tracking and motion forecasting with a single convolutional net. In *Proceedings of the IEEE Conference on Computer Vision and Pattern Recognition (CVPR)*, 2018.
- [15] Srikanth Malla, Behzad Dariush, and Chiho Choi. Titan: Future forecast using action priors, 2020.
- [16] Gregory P. Meyer, Jake Charland, Darshan Hegde, Ankit Laddha, and Carlos Vallespi-Gonzalez. Sensor fusion for joint 3D object detection and semantic segmentation. In *Proceedings of the IEEE Conference on Computer Vision and Pattern Recognition Workshops (CVPRW)*, 2019.
- [17] Gregory P. Meyer, Ankit Laddha, Eric Kee, Carlos Vallespi-Gonzalez, and Carl K. Wellington. LaserNet: An efficient probabilistic 3D object detector for autonomous driving. In *Proceedings of the IEEE Conference on Computer Vision and Pattern Recognition (CVPR)*, 2019.
- [18] Gregory P Meyer, Jake Charland, Shreyash Pandey, Ankit Laddha, Carlos Vallespi-Gonzalez, and Carl K Wellington. Laserflow: Efficient and probabilistic object detection and motion forecasting. *arXiv preprint arXiv:2003.05982*, 2020.
- [19] Anton Milan, S Hamid Rezatofighi, Anthony Dick, Ian Reid, and Konrad Schindler. Online multi-target tracking using recurrent neural networks. In *Thirty-First AAAI Conference on Artificial Intelligence*, 2017.
- [20] Nima Mohajerin and Mohsen Rohani. Multi-step prediction of occupancy grid maps with recurrent neural networks. *2019 IEEE/CVF Conference on Computer Vision and Pattern Recognition (CVPR)*, Jun 2019. doi: 10.1109/cvpr.2019.01085. URL <http://dx.doi.org/10.1109/CVPR.2019.01085>.
- [21] Jiquan Ngiam, Benjamin Caine, Wei Han, Brandon Yang, Yuning Chai, Pei Sun, Yin Zhou, Xi Yi, Ouais Alsharif, Patrick Nguyen, et al. Starnet: Targeted computation for object detection in point clouds. *arXiv preprint arXiv:1908.11069*, 2019.

- [22] Amir Sadeghian, Alexandre Alahi, and Silvio Savarese. Tracking the untrackable: Learning to track multiple cues with long-term dependencies. In *Proceedings of the IEEE International Conference on Computer Vision*, pages 300–311, 2017.
- [23] Amir Sadeghian, Ferdinand Legros, Maxime Voisin, Ricky Vesel, Alexandre Alahi, and Silvio Savarese. CAR-Net: Clairvoyant attentive recurrent network. In *Proceedings of the European Conference on Computer Vision (ECCV)*, 2018.
- [24] Marcel Schreiber, Stefan Hoermann, and Klaus Dietmayer. Long-term occupancy grid prediction using recurrent neural networks. *2019 International Conference on Robotics and Automation (ICRA)*, May 2019. doi: 10.1109/icra.2019.8793582. URL <http://dx.doi.org/10.1109/ICRA.2019.8793582>.
- [25] Samuel Schuster, Paul Vernaza, Wongun Choi, and Manmohan Chandraker. Deep network flow for multi-object tracking. In *Proceedings of the IEEE Conference on Computer Vision and Pattern Recognition*, pages 6951–6960, 2017.
- [26] Rudolph Van Der Merwe, Eric A Wan, et al. Sigma-point kalman filters for integrated navigation. In *Proceedings of the 60th Annual Meeting of the Institute of Navigation (ION)*, pages 641–654, 2004.
- [27] Bin Yang, Wenjie Luo, and Raquel Urtasun. PIXOR: Real-time 3D object detection from point clouds. In *Proceedings of the IEEE Conference on Computer Vision and Pattern Recognition (CVPR)*, 2018.
- [28] Wenyuan Zeng, Wenjie Luo, Simon Suo, Abbas Sadat, Bin Yang, Sergio Casas, and Raquel Urtasun. End-to-end interpretable neural motion planner. In *Proceedings of the IEEE Conference on Computer Vision and Pattern Recognition (CVPR)*, 2019.
- [29] Yin Zhou and Oncel Tuzel. VoxelNet: End-to-end learning for point cloud based 3D object detection. In *Proceedings of the IEEE Conference on Computer Vision and Pattern Recognition (CVPR)*, 2018.